Original paper

Characterization of mouse spinal cord vascular network by means of synchrotron radiation X-ray phase contrast tomography

Lorenzo Massimi [a,*], Michela Fratini [a,b], Inna Bukreeva [a,c], Francesco Brun [a], Alberto Mittone [d], Gaetano Campi [e], Raffaele Spanò [g], Milena Mastrogiacomo [g], Nicole Kerlero de Rosbo [f], Alberto Bravin [d], Antonio Uccelli [f], Alessia Cedola [a]

[a] Consiglio Nazionale delle Ricerche, Istituto di Nanotecnologia, Rome Unit, I-00195 Rome, Italy
[b] Fondazione Santa Lucia IRCCS, 00179 Roma, Italy
[c] P.N. Lebedev Physical Institute, Russian Academy of Sciences, Leninskii pr., 53 Moscow, Russia
[d] European Synchrotron Radiation Facility, F-38043 Grenoble, Cedex 9, France
[e] Institute of Crystallography-CNR, Monterotondo, Rome, Italy
[f] University of Genova DINOGMI Largo Daneo, 3 IT-16132 Genova, Italy
[g] Department of Experimental Medicine, University of Genova & AUO San Martino – IST Istituto Nazionale per la Ricerca sul Cancro, Largo R. Benzi 10, 16132 Genova, Italy

ARTICLE INFO

Article history:
Received 11 May 2016
Received in Revised form 24 July 2016
Accepted 22 September 2016
Available online 13 October 2016

Keywords:
Spinal cord vascular network
X-ray phase contrast tomography
Vascular segmentation

ABSTRACT

High resolution Synchrotron-based X-ray Phase Contrast Tomography (XPCT) allows the simultaneous detection of three dimensional neuronal and vascular networks without using contrast agents or invasive casting preparation. We show and discuss the different features observed in reconstructed XPCT volumes of the ex vivo mouse spinal cord in the lumbo-sacral region, including motor neurons and blood vessels. We report the application of an intensity-based segmentation method to detect and quantitatively characterize the modification in the vascular networks in terms of reduction in experimental visibility. In particular, we apply our approach to the case of the experimental autoimmune encephalomyelitis (EAE), i.e. human multiple sclerosis animal model.

1. Introduction

The role of the vascular network in several neurodegenerative diseases (e.g. amyotrophic lateral sclerosis, multiple sclerosis, Alzheimer's disease, Parkinson' disease) is currently under investigation. It is believed that a vascular damage represents the basis for a further progression of the disease up to the neuronal network insult [38,39,21]. In particular, for multiple sclerosis (MS) and its animal model, experimental autoimmune encephalomyelitis (EAE), an increased permeability of blood brain barrier or blood spinal cord barrier is observed, with subsequent infiltration of leukocytes in the central nervous system [22,20,2,13,10]. Consequent to a protracted local modification of the blood brain/spinal barrier, neuronal damage occurs, even though the underlying mechanisms are still to be elucidated [22,12]. In this framework, a quantification of the vascular insult plays an important role for the comprehension of the mechanism that drives neuronal damage in order to help the development of new therapeutic protocols [35].

To this aim, the extraction of the vascular map from tomographic images is required but the segmentation is hampered by the large variation of structural parameters involved when moving from larger arteries to smaller capillaries and by the low contrast between vessels and surrounding tissue. These make conventional (absorption) tomography unable to distinguish vessels. In order to overcome this limitation, the image contrast in conventional tomography is usually enhanced by using casting procedures or staining protocols in order to increase the absorption coefficient [27,17,32]. These procedures involve invasive preparations that introduce unwanted modifications in the vascular structures, especially if microvessels are considered [28]. More- over, in many pathologies discontinued vessels could be present, causing the contrast agent to spill out from the damaged vessel walls and leading to errors in quantification [7,28].

Synchrotron-based X-ray Phase Contrast Tomography (XPCT) provides an excellent investigation tool for soft tissues where conventional absorption tomography fails [4,30]. In particular, the mapping of the phase shift of the incident X-ray beam allows the simultaneous exploration of cellular and vascular distribution in biological samples without any casting preparation and with resolution in the 1–10 μm range [11]. Moreover, capability to

* Corresponding author.
E-mail address: lorenzo.massimi@uniroma1.it (L. Massimi).

distinguish vascular network without contrast agents has been already demonstrated, such as in the case of liver, tumors and central nervous system [25,19,33,11]. Even though the visual inspection of tomography data can be very useful, image segmentation is a crucial step for obtaining quantitative information. The purpose of any segmentation method is to classify the voxels of a particular feature in order to further assess significant parameters, thus providing a better visualization of the region of interest. Several approaches exist in order to reach this goal, including intensity and model-based algorithms [19,18,26,31].

In the present work we discuss a methodological approach to provide a quantitative measurement of vascular modification of mouse spinal cord. We previously examine different features observed in tomographic volume of the ex vivo mouse spinal cord in the lumbo-sacral region. Then we discuss the application of a simple intensity-based segmentation method to detect the vascular network. The proposed analysis is based on the image gray level histogram by considering the result of different threshold values. To better assess the spatial arrangement of the different features in the vascular network, 3D volume renderings of the segmented tomographic volumes are also presented. Finally, as preliminary study, we applied this method to a small sample of three healthy and EAE-affected (24 h from disease onset) mouse spinal cords to test its capability to detect modifications in the vascular network.

2. Material and methods

2.1. Sample preparation

Experimental animal procedures were carried out at the Animal Facility of the University of Genova (Genova, Italy), in the respect of the national current regulations regarding the protection of animals used for scientific purpose (D.Lgs 27/01/1992, n. 116). All animals were housed in pathogen-free conditions and treated according to the Italian and European guidelines (Decreto Legislativo 4 marzo 2014, n. 26, legislative transposition of Directive 2010/63/EU of the European Parliament and of the Council of 22 September 2010 on the protection of animals used for scientific purposes), with food and water ad libitum. The research protocol was approved by the Ethical Committees for Animal Experimentation of the University of Genoa (No. 319). We studied the spinal cord of three healthy C57 Black mice and three EAE-affected mice. Female 6–8 week-old C57Bl/6 J mice (18–20 g) were immunized for EAE as described by subcutaneous injection at two sites in the flank with an emulsion of 200 μg myelin oligodendrocyte glycoprotein (MOG) peptide 3555 (Espikem) in incomplete Freund adjuvant (IFA; Difco) containing 300 g Mycobacterium tuberculosis (strain H37Ra; Difco). Mice were injected in the tail vein with 400 ng pertussis toxin (Sigma–Aldrich) immediately and 48 h after immunization. The mice were scored daily for clinical manifestations of EAE on a scale of 0–5 [24]. We studied the spinal cord of healthy and EAE-affected mice. For the XPCT experiments mice were perfused transcardially with saline solution containing heparin (50 U/ml). Spinal cords were dissected out, fixed in 4% paraformaldehyde for 24 h, and maintained in 70% alcohol until analysis. Before the XPCT experiments mice underwent laminectomy and the spinal cord was taken off, dehydrated using graded ethanol and immersed in methyl salicylate for 24–48 h. Finally, it has been embedded in agar.

2.2. Experimental

Phase shift detection has been carried out using free space propagation setup. X-rays propagates through the sample and refraction of the X-ray beam from its original path is observed if sample density locally changes. Generally, if the detector is placed close enough to the sample, such as in conventional absorption tomography, these variations are not detected. On the other hand, when a long enough space between sample and detector is left, refracted light can prop- agate in the free space and interfere if a sufficient degree of coherence is provided [9]. Thus, the final recorded image contains information about different densities in the sample in the form of interference fringes. In view of the high photon flux, monochromatic beams and high degree of coherence, synchrotron radiation can provide all conditions to obtain high spatial resolution phase contrast images. XPCT measurements were performed at the ID 17 beamline of European Synchrotron Radiation Facility (ESRF) in Grenoble (France) [5]. Monochromatic X-ray beam at the energy of 30 keV was used in combination with a sample-detector distance of 2.3 meters and a detector pixel size of 3.5 μm. The tomography data was acquired in half acquisition mode with 4000 projections covering a total angle range of 360 and an acquisition time of 1 s per projection. Phase retrieval was performed using a single distance method developed by Paganin [29]. Image analysis were carried out by means of ImageJ software and 3D rendering representations were generated using VG Studio Max 2.0 (Volume Graphics, Heidelberg, Germany).

3. Results

In order to discuss the different features detectable in tomographic slices, we report in Fig. 1(a–c) the minimum and in Fig. 1(d–f) the maximum values across all tomographic slices in a reconstructed transverse and sagittal cross Section (0.5 mm thick volume) in the lumbo-sacral region of an healthy mouse spinal cord.

Due to the lower density of vessel lumen compared to the surrounding tissue, the vascular network appears as a dark feature in the minimum of the tomographic volume. On the other hand, in the maximum of the tomographic volume we observe structures compatible with vessel walls and neuronal cells due to the higher density as compared to the surrounding tissue (Fig. 1d). In particular, in the transverse section we can distinguish the typical H shape of the gray matter, the central (sulcal) vasculature, marked with red arrow in Fig. 1a and the vessels entering radially in the white matter, indicated by red arrows in Fig. 1b [16,6,36,34]. In the sagittal view (Fig. 1c), the central vascularization bifurcation in the ventral spinal cord region is clearly visible [16,23,6,36,37,34]. In Fig. 1(d and e) it is possible to clearly distinguish cells compatible with motor neurons on the ventral horn, which appear as bright spots (see white arrows) [18,29]. Interesting features are also observed at the gray/white matter interface: a complex network of fibers radially distributed (see light blue arrow in Fig. 1e), in agreement with the presence of nervous fibers in this region [11,16,6,36,37,34].

Because of the high quality of the resulting images, we were able to perform an intensity-based segmentation analysis of the vascular network. In Fig. 2a, three selected slices of 3.5łμm thickness are reported with the histogram of the whole volume. Moreover, to evaluate different features included in segmentation, we report in Fig. 2b the two-dimensional projection of the segmented voxels at different gray levels marked in the histogram, overlapped with the minimum and maximum of tomographic volume, respectively.

In intensity-based segmentation approach, the fundamental step is represented by determination of a reasonable threshold value in the gray level histogram of the image. In order to define a quantitative reference for the thresholding, we empirically deconvolve the histogram curve of the whole tomographic volume with three different components around the modal value, associ-

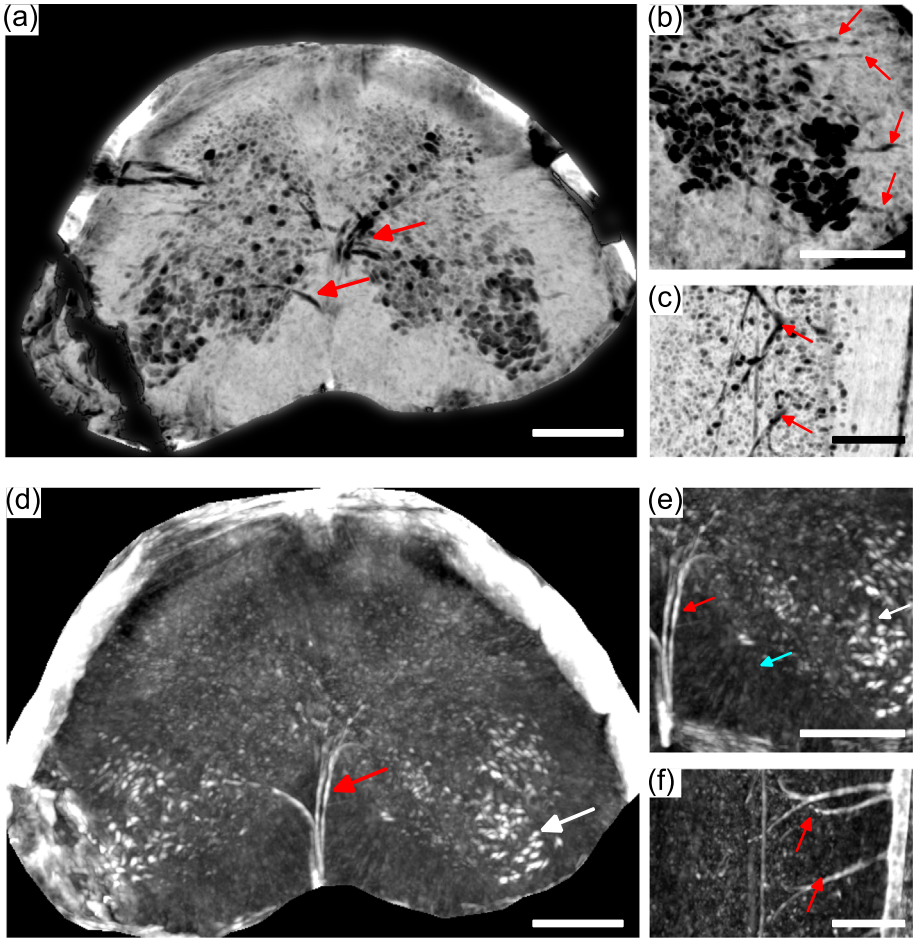

Fig. 1. (a) and (b) minimum of reconstructed transverse cross Section (0.5 mm thick) combined with details in a region of interest. Red arrows point to the ramifications of central (sulcal) vasculature. (c) sagittal cross section of the reconstructed volume. Red arrows highlight the bifurcation of central vascularization. (d) and (e) maximum of reconstructed transverse cross Section (0.5 mm thick) combined with details in a region of interest. Red and white arrows point at higher density features compatible with vessel wall of central vascularization and motor neurons, respectively. Light blue arrow highlights nervous fibers radially distributed. (f) maximum of sagittal cross section of reconstructed volume. Red arrows point at same features reported in (d) and (e), compatible with vessel walls. Scale bar is 300 μm. (For interpretation of the references to colour in this figure legend, the reader is referred to the web version of this article.)

ated to different gray levels corresponding to different detectable features in the sample, as described in Fig. 2. The voxels of the vascular network have a darker gray level with respect to the surrounding tissue; as a result, they are located on the left tail of the image histogram. This is confirmed by the image shown in Fig. 2b$_1$, which is only based on the voxels characterized by a gray level lower than the threshold labeled as b$_1$ in Fig. 2b and includes a large amount of the vascular area. Moreover, the presence of asymmetric tail on the left part of the histogram is easily observed in logarithmic plot. An increase of the gray threshold value up to the position of the center of the first peak (b$_2$ threshold) results in the inclusion of many more voxels in the positions surrounding the vessels' lumens, which cannot be unambiguously assigned to vascularization (see Fig. 2b$_2$). The second peak can be easily identified as the one centered onto the modal value of the whole histogram, and specifically with the dominant gray value of the whole image, which represents tissue surrounding the spinal cord parenchyma. The visualization of the gray levels that comprise the second peak can be accomplished by considering the appropriate threshold value, labeled as b$_3$ in Fig. 2b. As displayed in Fig. 2b$_3$, this range includes a large amount of voxels that are not compatible either with lumens or with vessel walls, and therefore have to be rejected. A similar analysis can be performed for the right part of the histogram, where voxels compatible with vessel walls and cellular bodies are expected. The presence of an asymmetric tail on the right side of the histogram (clearly visible in the logarithmic plot shown in Fig. 2b) is taken into account by introducing a small peak on the right of the main one, and by using it as a reference in the determination of the threshold levels. For the b$_4$ threshold value, voxels belonging to cellular bodies and compatible with vessels walls are included (Fig. 2b$_4$). The increase of the threshold to the position of the center of the small peak (see Fig. 2b$_5$) and beyond (Fig. 2b$_6$), includes unwanted voxels from the surrounding tissue.

The analysis summarized in Fig. 2 allows us to visually identify the optimal threshold levels for separately visualizing the vessel network (threshold b$_1$, see Fig. 2b$_1$) and the surrounding tissues (threshold b$_4$, see Fig. 2b$_4$). After applying these thresholds, a 3D rendering of the tomographic volume can be performed in order to better visualize the vascular distribution. An example according to two different viewing angles is shown in Fig. 3.

The empty space of central canal is well rendered (see white arrow in Fig. 3). In addition, anterior spinal vessels are evident and run along the whole tomographic volume in two different features with opposite contrast (white asterisk in Fig. 3). Central vessels, originated from the anterior spinal vessels, penetrate the median fissure with a slight tilt with respect to the transverse cross section and branch at the height of central canal (see red arrows) [16,23,6,36,37,34]. Finally, the green arrow shows a disconnection in the blood vessel due to a local decrease of contrast.

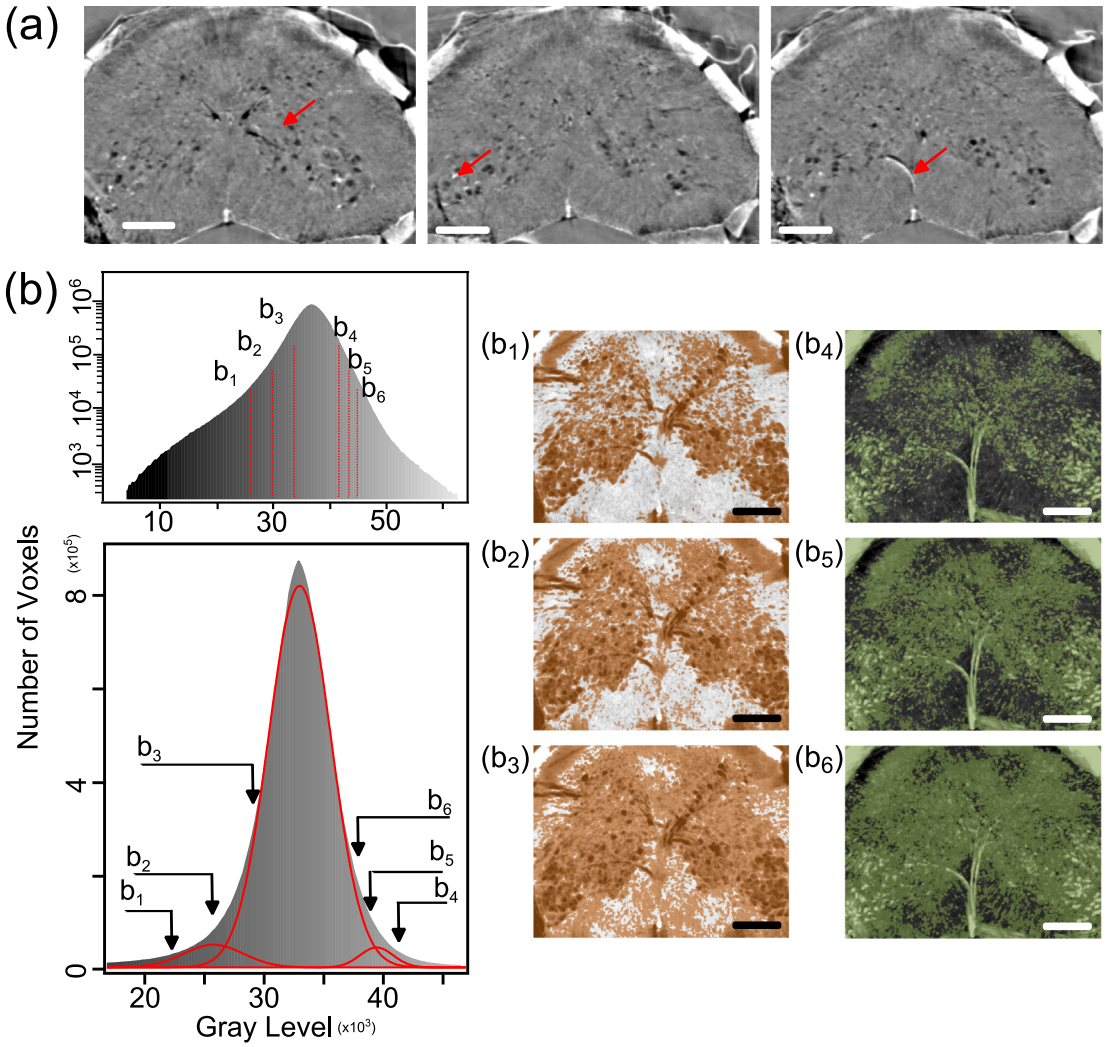

Fig. 2. (a) three selected tomographic slices at different sample depth; voxel size is 3.5 × 3.5 × 3.5 μm. From left to right red arrows indicates vascularization in gray matter, motor neurons and central vessel, respectively. (b) the histogram of whole tomography volume in logarithmic (top panel) and linear scale (bottom panel) are reported with the two-dimensional projection of segmented voxels overlapped with the minimum and maximum of tomographic volume at different gray levels marked in the histograms, from b_1 to b_6. Scale bar is 300 μm. (For interpretation of the references to colour in this figure legend, the reader is referred to the web version of this article.)

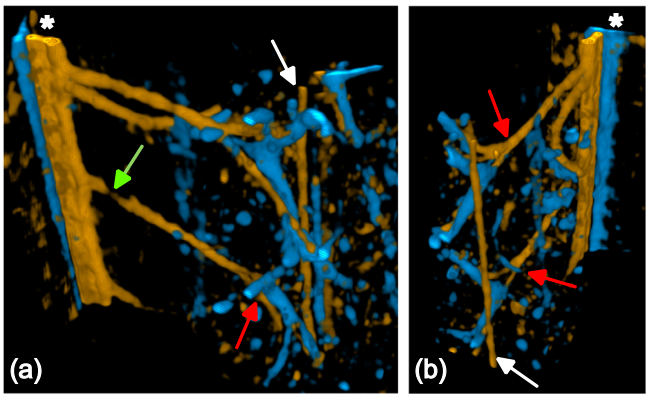

Fig. 3. (a) and (b) 3D rendering, at different viewing angles, of main vascularization (0.5 mm thick volume) including anterior spinal vessels (white asterisk) and central vessels penetrating the spinal cord and branching (red arrows) at the height of central canal (white arrows). The green arrow shows a disconnection in the blood vessel due to a segmentation artifact. (For interpretation of the references to colour in this figure legend, the reader is referred to the web version of this article.)

In order to test the sensitivity of the segmentation procedure to detect alterations in vascular network, we compare the healthy case with EAE-affected mice (24 h from disease onset), see Fig. 4. We report a 3D rendering of the vascular network in a tomographic volume (0.5 mm thick) in the healthy and diseased case. In addition, we show the minimum of reconstructed transverse cross section of half of the spinal cord.

From a qualitative point of view, the decrease of vascular features is well observed in the 3D rendering. The comparison of healthy and EAE-affected mouse reveals a decrease in vascular features. In addition, the minimum of tomographic volume shows a decrease in surface occupied by vascularization due to a decreasing in its visibility, in agreement with the expected role of vascular insult in the development of the disease [22,20,2,13,10]. In order to quantify vascular changes the ratio between the volume occupied by voxels assigned to vessels lumen and the total sample volume has been considered in a preliminary sample of three healthy and EAE affected mice. In healthy mice, an average percentage ratio between total and vascular volume of $(1.8 \pm 0.3)\%$ was found in comparison with a ratio of $(0.7 \pm 0.3)\%$ in EAE-affected mice as

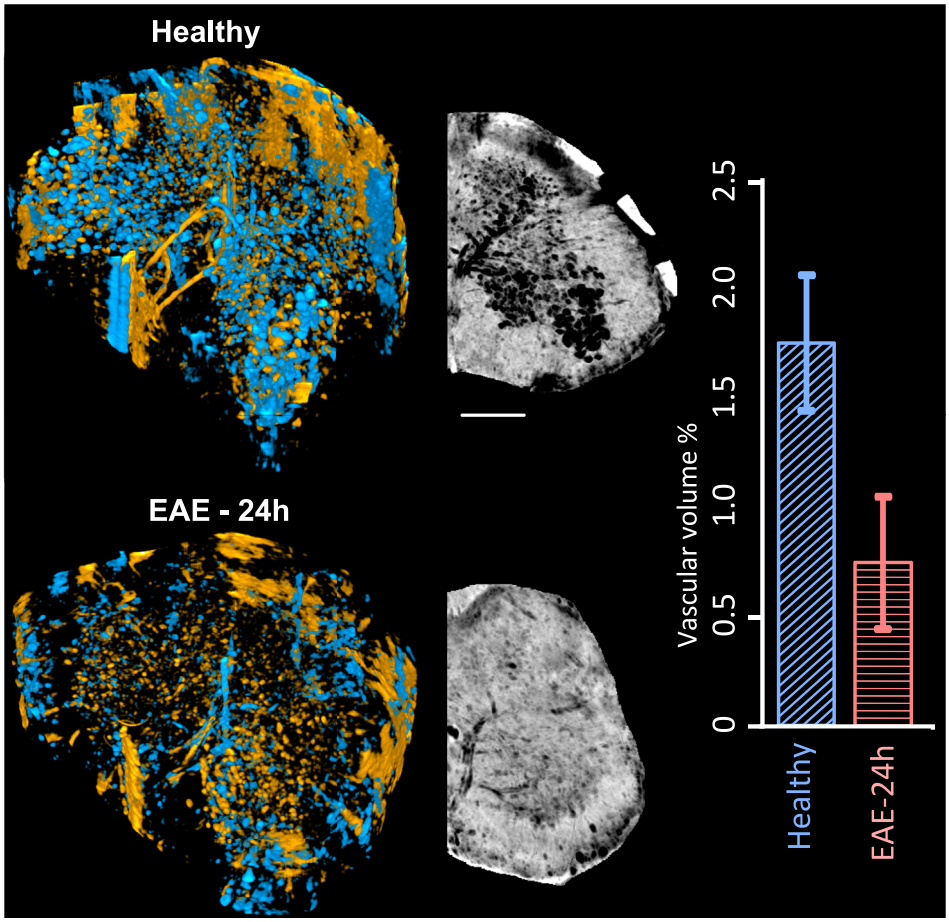

Fig. 4. Comparison between the healthy and diseased lumbar segmented tomographic volume. 3D rendering and minimum of the volume on left and right, respectively. Voxel size is $3.5 \times 3.5 \times 3.5\ \mu m^3$. A reduction in visibility of vessels lumen can be observed. Scale bar is 300 μm for all images. Histogram with average percentage volume with absolute error is also reported considering a preliminary set of three mice for each class.

shown in the histogram in Fig. 4, demonstrating the capability of this simple segmentation procedure to detect modifications in vascular network.

4. Discussion

Synchrotron-based XPCT is capable to simultaneously image the vascular and neuronal network in mouse spinal cord, providing possibility to study the complex interplay between them [11]. In particular, as reported in Fig. 1, we are able to image motor neuron soma located in the ventral horn together with vessels lumen. Moreover, we are able to detect both the vascularization in the gray matter, originated from anterior spinal vessels, and the radial vascularization, entering radially in the white matter [16,6,36,37,34].

Thanks to the analysis of the image histogram, reported in Fig. 2, intensity-based segmentation has been used in this study to extract voxels assigned to vessels. In particular, the image histogram is characterized by a mono-modal distribution with slightly asymmetric tails on both sides of the modal value. It is easy to recognize that the main peak, shown in Fig. 2b, is assigned to all the tissue surrounding spinal cord parenchyma and it has not to be included in the segmented volume. On the other hand, voxels compatible with vessel lumen or walls and motor neurons have to be included and are located on gray levels identified by two small peaks at both sides of the main one, respectively. The result of the threshold application to the whole tomographic volume is shown in Fig. 3. Segmentation is able to reproduce the central vascularization with a good degree of accuracy. In particular, two central vessels can be easily seen, which are compatible with the anterior spinal artery and vein [16,6,36,37,34]. Unfortunately, the usage of a simple intensity approach presents several drawbacks. Since no assumption on the continuity of the detected structure is considered, voxels with a local contrast decrease will not be included even though they represent part of the vessel. This is clearly observed in Fig. 3 (see green arrow), where a local decrease of the intensity splits a single vessel in two different branches introducing a false branch. In order to overcome this limitation undecided voxels can be attached to segmented ones using different approaches [3,14]. Despite some limitations, intensity-based segmentation provides a good starting point to obtain fast and quantitative results. We tested the segmentation procedure on a small sample of three healthy and EAE-affected mice respectively. A comparison is reported in Fig. 4 showing the minimum and 3D rendering of the tomographic volume. In particular, to provide a statistical estimator for alterations in vascular network we considered the ratio between the number of voxels assigned to vascular network and the total number of the voxels of the tomographic spinal cord volume. This approach provides a reasonable quantification of vascular modifications if a decrease of the experimental visibility of the vessels is present (e.g vessel lumen occlusions) such as qualitatively observed in our case. However, it can fail when only a rearrangement of vascular network is present maintaining the total vascular volume constant. In order to test our approach we compared a small sample of healthy and

EAE-affected mice. In the EAE, we observe a modification in the volume occupied by vascularization due to a diminished visibility of vessels with XPCT. Despite XPCT is not capable to provide information about pathological conditions of EAE at microscopic level, we observe that the reduction of visibility of the vascular network is compatible with modifications of blood vessels as a consequence of inflammatory response to infiltration of immune cells, already observed in human multiple sclerosis and animal model [8,1,15].

5. Conclusions

In this work we used synchrotron-based XPCT to investigate the vascularization of ex vivo mouse spinal cord at the lumbo-sacral region. XPCT provides a simultaneous view of the vascular and neuronal networks without the adoption of casting procedures or contrast agents. We discussed the use of the intensity-based segmentation approach to extract voxels assigned to vessels for providing a quantification of the alterations in the vascular network. This approach presents several limitations and drawbacks, especially if an assessment of the vessels'diameter is further required. Despite the limitations, it provides a good representation of vascular network of the spinal cord as shown by 3D rendering. Finally, we tested the capacity of this segmentation method to detect alterations in the central nervous system vascular network between healthy and EAE-affected mice. We observed a substantial decrease in the vascular volume, in agreement with the presence of vascular alteration in the early phase of the disease. From a pathological point of view we observed a decrease tendency in the vascularization volume, in agreement with the presence of vascular alteration in the early phase of the EAE disease. The decrease in the vascularization appears as a weaker detectable contrast in the recorded image of the vessels. The obtained results pave the way for a systematic investigation of the vascular alterations in neurodegenerative disease. In particular the comparison between different neurological scores may be monitored and new advanced therapies based on stamina cells can be tested.

Acknowledgement

Authors thank the ID17 beamline at the ESRF for the provision of beamtime and the beamline staff for the experimental support. The European project VOXEL "Volumetric Medical X-ray Imaging at extremely low dose" (HORIZON 2020-FET Open; Project reference: 665207) is acknowledged for financial support. The Italian Ministry of Health Young Researcher Grant 2013 (GR-2013-02358177) is also acknowledged for financial support by MF. The COST Action MP1203 "Advanced X-ray spatial and temporal metrology" are acknowledged for networking support.

References

[1] Adams RA, Passino M, Sachs BD, Nuriel T, Akassoglou K. Fibrin mechanisms and functions in nervous system pathology. Mol Interv 2004;4(3):163.
[2] Arima Y, Harada M, Kamimura D, Park JH, Kawano F, Yull FE, et al. Regional neural activation defines a gateway for autoreactive t cells to cross the blood-brain barrier. Cell 2012;148(3):447–57.
[3] Atwood RC, Lee PD, Konerding MA, Rockett P, Mitchell CA. Quantitation of microcomputed tomography-imaged ocular microvasculature. Microcirculation 2010;17(1):59–68.
[4] Bonse U, Busch F. X-ray computed microtomography (μct) using synchrotron radiation (sr). Prog Biophys Mol Biol 1996;65(1):133–69.
[5] Bravin A, Coan P, Suortti P. X-ray phase-contrast imaging: from pre-clinical applications towards clinics. Phys Med Biol 2012;58(1):R1.
[6] Cao Y, Wu T, Li D, Ni S, Hu J, Lu H, et al. Three-dimensional imaging of microvasculature in the rat spinal cord following injury. Sci Rep 2015;5:12643.
[7] Carmeliet P, Jain RK. Angiogenesis in cancer and other diseases. Nature 2010;407(6801):249–57.
[8] Davalos D, Ryu JK, Merlini M, Baeten KM, Le Moan N, Petersen MA, et al. Fibrinogen-induced perivascular microglial clustering is required for the development of axonal damage in neuroinflammation. Nat Commun 2012;3:1227.
[9] Di Fonzo S, Jark W, Soullie G, Cedola A, Lagomarsino S, Cloetens P, et al. Submicrometre resolution phase-contrast radiography with the beam from an x-ray waveguide. J Synchrotron Radiat 1998;5(3):376–8.
[10] Errede M, Girolamo F, Ferrara G, Strippoli M, Morando S, Boldrin V, et al. Blood-brain barrier alterations in the cerebral cortex in experimental autoimmune encephalomyelitis. J Neuropathol Exp Neurol 2012;71(10):840–54.
[11] Fratini M, Bukreeva I, Campi G, Brun F, Tromba G, Modregger P, et al. Simultaneous submicrometric 3d imaging of the micro-vascular network and the neuronal system in a mouse spinal cord. Sci Rep 2016;5:8514.
[12] Ge Y, Zohrabian VM, Grossman RI. Seven-tesla magnetic resonance imaging: new vision of microvascular abnormalities in multiple sclerosis. Arch Neurol 2008;65(6):812–6.
[13] Giunti D, Borsellino G, Benelli R, Marchese M, Capello E, Valle MT, et al. Phenotypic and functional analysis of t cells homing into the csf of subjects with inflammatory diseases of the cns. J Leukoc Biol 2003;73(5):584–90.
[14] Huo YK, Wei G, Zhang YD, Wu LN. An adaptive threshold for the canny operator of edge detection. 2010 International Conference on Image Analysis and Signal Processing. IEEE; 2010. p. 371–4.
[15] Koh CS, Gausas J, Paterson PY. Neurovascular permeability and fibrin deposition in the central neuraxis of lewis rats with cell-transferred experimental allergic encephalomyelitis in relationship to clinical and histopathological features of the disease. J. Neuroimmunol 1993;47(2):141–5.
[16] Koyanagi I, Tator CH, Lea PJ. Three-dimensional analysis of the vascular system in the rat spinal cord with scanning electron microscopy of vascular corrosion casts. part 1: normal spinal cord. Neurosurgery 1993;33(2):277–84.
[17] Krucker T, Lang A, Meyer EP. New polyurethane-based material for vascular corrosion casting with improved physical and imaging characteristics. Microsc Res Tech 2006;69(2):138–47.
[18] Lang S, Dominietto M, Cattin P, Ulmann-Schuler A, Weitkamp T, Mueller B. Global and local hard X-ray tomography of a centimeter-size tumor vessel tree. J Synchrotron Radiat 2012;19(1):114–25.
[19] Lang S, Müller B, Dominietto MD, Cattin PC, Zanette I, Weitkamp T, et al. Three-dimensional quantification of capillary networks in healthy and cancerous tissues of two mice. Microvasc Res 2012;84(3):314–22.
[20] Larochelle C, Alvarez JI, Prat A. How do immune cells overcome the blood–brain barrier in multiple sclerosis? FEBS Lett 2011;585(23):3770–80.
[21] Maragakis NJ, Rothstein JD. Mechanisms of disease: astrocytes in neurodegenerative disease. Nat Clin Pract Neurol 2006;2(12):679–89.
[22] McFarland HF, Martin R. Multiple sclerosis: a complicated picture of autoimmunity. Nat Immunol 2007;8(9):913–9.
[23] Melissano G, Bertoglio L, Rinaldi E, Leopardi M, Chiesa R. An anatomical review of spinal cord blood supply. J Cardiovasc Surg 2015;56(5):699–706.
[24] Mendel I, de Rosbo NK. Ben-Nun A.A myelin oligodendrocyte glycoprotein peptide induces typical chronic experimental autoimmune encephalomyelitis in h-2b mice: fine specificity and t cell receptor vβ expression of encephalitogenic t cells. Eur J Immunol 1995;25(7):1951–9.
[25] Momose A, Takeda T, Itai Y. Blood vessels: depiction at phase-contrast x-ray imaging without contrast agents in the mouse and rat-feasibility study. Radiology 2000;217(2):593–6.
[26] Müller B, Beckmann F, Huser M, Maspero F, Székely G, Ruffieux K, et al. Non-destructive three-dimensional evaluation of a polymer sponge by micro-tomography using synchrotron radiation. Biomol Eng 2002;19(2):73–8.
[27] Müller B, Fischer J, Dietz U, Thurner PJ, Beckmann F. Blood vessel staining in the myocardium for 3d visualization down to the smallest capillaries. Nucl Instr Meth Phys Res B 2006;246(1):254–61.
[28] Müller B, Lang S, Dominietto M, Rudin M, Schulz G, Deyhle H, et al. High-resolution tomographic imaging of microvessels. Optical Engineering + Applications. International Society for Optics and Photonics; 2008. p. 70780B.
[29] Paganin D, Gureyev TE, Pavlov KM, Lewis RA, Kitchen M. Phase retrieval using coherent imaging systems with linear transfer functions. Opt Commun 2004;234(1):87–105.
[30] Pelliccia D, Sorrentino A, Bukreeva I, Cedola A, Scarinci F, Ilie M, et al. X-ray phase contrast microscopy at 300 nm resolution with laboratory sources. Opt Express 2010;18(15):15998–6004.
[31] Pham DL, Xu C, Prince JL. Current methods in medical image segmentation 1. Annu Rev Biomol Eng 2000;2(1):315–37.
[32] Plouraboué F, Cloetens P, Fonta C, Steyer A, Lauwers F, Marc-Vergnes JP. X-ray high-resolution vascular network imaging. J Microsc 2004;215(2):139–48.
[33] Takeda T, Momose A, Wu J, Yu Q, Zeniya T, Yoneyama A, et al. Vessel imaging by interferometric phase-contrast x-ray technique. Circulation 2002;105(14):1708–12.
[34] Thron AK. Vascular anatomy of the spinal cord: neuroradiological investigations and clinical syndromes. Springer-Verlag; 2000.
[35] Uccelli A, Moretta L, Pistoia V. Mesenchymal stem cells in health and disease. Nat Rev Immunol 2008;8(9):726–36.
[36] Watson C. The mouse nervous system. Academic Press; 2012.
[37] Watson C, Paxinos G, Kayalioglu G. The spinal cord: a Christopher and Dana Reeve Foundation text and atlas. Academic press; 2009.
[38] Zlokovic BV. The blood-brain barrier in health and chronic neurodegenerative disorders. Neuron 2008;57(2):178–201.
[39] Zlokovic BV. Neurovascular pathways to neurodegeneration in alzheimer's disease and other disorders. Nat Rev Neurosci 2011;12(12):723–38.